

Shock-Wave Mach-Reflection Slip-Stream Instability: A Secondary Small-Scale Turbulent Mixing Phenomenon

A. Rikanati

Department of Physics, Ben Gurion University, Beer-Sheva 84015, Israel

O. Sadot

*Department of Mechanical Engineering, Ben Gurion University, Beer-Sheva 84015, Israel,
and Department of Physics, Nuclear Research Center, Negev 84190, Israel*

G. Ben-Dor

Department of Mechanical Engineering, Ben Gurion University, Beer-Sheva 84015, Israel

D. Shvarts

*Department of Physics, Ben Gurion University, Beer-Sheva 84015, Israel,
Department of Mechanical Engineering, Ben Gurion University, Beer-Sheva 84015, Israel,
and Department of Physics, Nuclear Research Center, Negev 84190, Israel*

T. Kuribayashi and K. Takayama

*Interdisciplinary Shock-Wave Research Center, Institute of Fluid Science, Tohoku University, Sendai, Japan
(Received 15 December 2005; published 3 May 2006)*

Theoretical and experimental research, on the previously unresolved instability occurring along the slip stream of a shock-wave Mach reflection, is presented. Growth rates of the large-scale Kelvin-Helmholtz shear flow instability are used to model the evolution of the slip-stream instability in ideal gas, thus indicating secondary small-scale growth of the Kelvin-Helmholtz instability as the cause for the slip-stream thickening. The model is validated through experiments measuring the instability growth rates for a range of Mach numbers and reflection wedge angles. Good agreement is found for Reynolds numbers of $Re > 2 \times 10^4$. This work demonstrates, for the first time, the use of large-scale models of the Kelvin-Helmholtz instability in modeling secondary turbulent mixing in hydrodynamic flows, a methodology which could be further implemented in many important secondary mixing processes.

DOI: [10.1103/PhysRevLett.96.174503](https://doi.org/10.1103/PhysRevLett.96.174503)

PACS numbers: 47.20.Lz, 47.20.Ft, 47.40.Nm, 47.63.mc

Understanding secondary turbulent mixing in complex unstable hydrodynamic flows is of great importance in achieving gain in laser driven inertial confinement fusion (ICF) as well as in many astrophysical processes [1–3]. Mach reflections (MRs) are a well known shock-wave related phenomenon occurring when an oblique shock wave reflects from a rigid wall (or interacts with a second shock wave) and are of great importance in many hydrodynamic flows [4]. The basic feature of a Mach reflection is that of the three shocks structure, giving rise to the slip-stream (SS) instability. In this Letter, we show, for the first time, that the growth of the SS instability is due to secondary turbulent mixing. Through modeling this instability, as described further on in this Letter, we implement a new technique for understanding secondary turbulent mixing, a technique which could be further implemented for many other hydrodynamic flows.

The MR three shocks structure is a phenomenon widely demonstrated in many experimental works (see [4] for examples), as well as in the example from the current work illustrated in Fig. 1 (see figure caption for details). The three shocks structure appears when the inclination angle, between the incident shock and the bounding wall, is

smaller than a critical angle defined through the detachment criteria [5], depending on the shock-wave Mach number and the material equation of state (see [4] and references therein for further details). In the MR structure, the SS is of a unique hydrodynamic nature, being a discontinuity which is not a shock. The SS separates between two regions (regions 2 and 3 in Fig. 1) of different densities ($\rho_2 \neq \rho_3$) and tangential velocities ($v_2^{\parallel} \neq v_3^{\parallel}$) but of equal pressures ($p_2 = p_3$) and of zero perpendicular velocities ($v_2^{\perp} = v_3^{\perp} = 0$), i.e., a shear flow. As can be seen from Fig. 1, and in contrast with the sharp nature of the three shock waves, the SS discontinuity thickness increases downstream from the triple point. To our knowledge, the full nature of this experimentally observed phenomenon, known as the SS instability, is still unresolved, with the leading assumption for the cause for this instability relating to the viscosity generated boundary layer effect [4].

As is the case in the SS discontinuity, the Kelvin-Helmholtz (KH) shear flow instability [6] occurs when two fluids flow with proximity to each other with a tangential velocity difference, defined as the shear velocity. Under this instability, small perturbations on the two fluid interface evolve into a formation of vortices causing the two

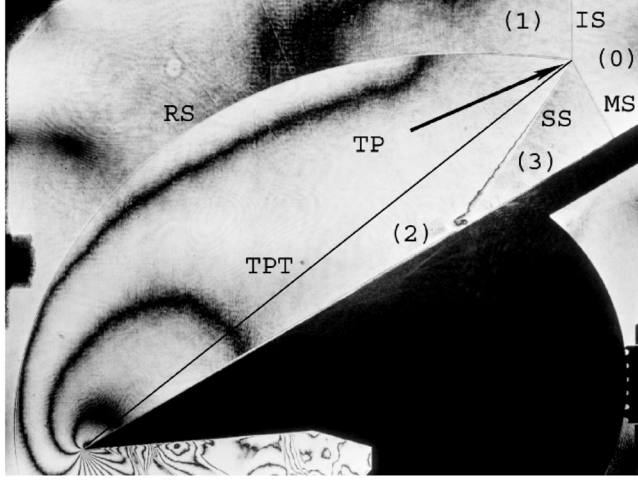


FIG. 1. A holographic interferometry image of a $M = 1.9$ Mach reflection in air with a wedge angle of $\theta_w = 30^\circ$ (see text for further experimental details). Marked are the following features: the incident shock (IS), the Mach stem (MS), the reflected shock (RS), the triple point (TP), the slip stream (SS), and the triple-point trajectory (TPT) which is also indicated by a dashed line. Four flow regions are distinguished: the non-shocked air (0), the shocked air above the reflection (1), the shocked air after the reflection (2), and the Mach-stem shocked air, before the SS (3).

fluids to turbulently mix. In this Letter, we demonstrate that the cause for the SS thickening is the KH instability evolving on the two fluid interface, generating secondary small-scale turbulent mixing.

The KH instability large-scale behavior has been thoroughly investigated through a wide range of experimental, numerical, and theoretical work resulting in an understanding of its growth rates and characteristics and of the main mechanisms dominating its evolution (see, for example, [6,7]). By implementing previously reported KH large-scale instability growth rates [6,7], we try to model the spread angle of the SS instability as a function of the MR flow parameters. In the following paragraphs, a brief description of the growth rates of the large-scale KH instability will be presented, followed by a detailed modeling of the SS instability evolution. The model predictions are then verified through comprehensive experimental research. Finally, a short description of viscous effects and the relation to the Re number of the flow is presented, again supported by experimental results.

Apart from revealing the nature of this previously unresolved phenomenon (the SS instability), the success of the process described in this Letter demonstrates, for the first time, that large-scale models of the KH instability can be implemented in describing secondary turbulent mixing in hydrodynamic flows. Similar methodologies could be further implemented to many other phenomena involving secondary mixing, such as the ICF relevant Rayleigh-Taylor and Richtmyer-Meshkov instabilities [2,3]. It should be mentioned that an attempt to numerically de-

scribe secondary mixing phenomena through the solution of full 2D or 3D Euler equations is expected to be very difficult, if not impossible. That is due to the very large number of computational cells required to describe both the large-scale and the small-scale mixing processes.

As expected from dimensional considerations, the width of the KH large-scale turbulent mixing zone (TMZ) evolves with time according to $\delta h(t) = c\Delta v t$, where Δv is the shear velocity, t represents the evolution time, and $c = 0.19 \pm 0.01$ is a dimensionless constant derived experimentally [6], numerically, and recently even theoretically [7]. It should be mentioned that, in most experiments, the instability growth is measured spatially, i.e., as a function of the advection distance from the mixing starting point. The spatial mixing growth rate is easily related to the temporal growth by assuming the average flow flows downstream with the fluid average velocity, resulting in $\delta h(x) = 2c[(v_1 - v_2)/(v_1 + v_2)]x$, where v_1 and v_2 are the two fluid velocities and c is the previously mentioned dimensionless constant. To this equation, two corrections must be introduced. The first, as reported in Ref. [7], is for cases of fluids of two different densities, and the second is for high Mach number flows ($\frac{\Delta v}{a} > 1$, where a is the fluid average sound speed). Following these two corrections, the TMZ width $\delta h(x)$ becomes

$$\delta h(x) = (0.38 \pm 0.02) \frac{S(v_1, v_2)}{1 - 2f_d(\rho_1/\rho_2)S(v_1, v_2)} \times x f_{\text{HiMach}}\left(\frac{\Delta v}{a}\right); \quad (1)$$

$$f_d(\rho_1, \rho_2) = \frac{1}{2} \left| \frac{1 - \sqrt{\rho_2/\rho_1}}{1 + \sqrt{\rho_2/\rho_1}} \right|,$$

where $S(v_1, v_2) = (v_1 - v_2)/(v_1 + v_2)$. $f_{\text{HiMach}}(\frac{\Delta v}{a}) = 0.5(1 - \tanh(2(\frac{\Delta v}{a} - 1.2)))$ is the high Mach correction which is based on a parametric fit of the results shown in Ref. [8]. Finally, based on Eq. (1), the spread angle of the spatially growing instability is found according to

$$\theta_{\text{spread}} = \arctan\left(\frac{\delta h(x)}{2x}\right). \quad (2)$$

When trying to implement Eq. (2) for the growth of the SS instability, one needs to describe v_1 , v_2 , ρ_1 , and ρ_2 of the two fluids along the SS. These physical properties are the velocities (in the frame of reference moving with the triple point) and the densities of regions 2 and 3 in Fig. 1. All are analytically calculated using the three-shock theory first suggested by von Neumann [5]. The theory is based on the traditional shock-wave conservation equations which are implemented for a single oblique shock. For an ideal gas (see [9]), the flow parameters behind an oblique shock can be analytically derived through a set of analytical translation functions, as a function of the shock inclination angle and the preshock conditions. By implementing these translation functions 3 times, once for each shock in the

three-shock complex, and by demanding the closure relations of pressure equalization between regions 2 and 3, $P_2 = P_3$, and zero perpendicular velocity, $v_2^\perp = v_3^\perp = 0$, the flow parameters can be solved in the entire domain. By additionally assuming that the Mach stem is perpendicular to the wedge, one can also find the angle of the triple-point trajectory. Once the flow parameters are known, the four physical parameters mentioned above are easily obtained. It can be shown from the translation function mentioned earlier that the resulting spread angle depends only on the incident shock-wave Mach number, the reflecting wedge angle, and the adiabatic index of the gas γ , while the initial density and pressure are of no importance. In Fig. 2, one can see the resulting SS instability spread angles for MR in air ($\gamma = 1.4$) as a function of the incident shock-wave Mach number for reflecting wedge angles of $\theta_w = 20^\circ, 30^\circ, 40^\circ, 45^\circ$.

Notice that, initially, the expected spread angle increases with the increase in Mach number or wedge angle, until a value of about 8° , after which the spread angle decreases. This effect is a result of the Mach number reduction factor of Eq. (1).

In order to verify the model predictions, complementary experimental research was conducted using a shock-tube facility at the Interdisciplinary Shock-Wave Research Center of the Institute of Fluid Science, Tohoku University. The tube allows the generation of Mach 1.1–5 shock waves passing through a rectangular tube with a 10 cm by 18 cm cross section. Near the end of the tube, a windowed test

section allows the user to implement optical diagnostics. A steel wedge with a varying angle was placed in the test section, and holographic interferometry images were taken of the MR generated from the shock-wedge interaction. For further details on the shock tube and the interferometry technique, see [10]. Experiments were done with ambient air at an initial pressure of $P_0 = 10.1$ kPa, wedge angles of $\theta_w = 20^\circ, 30^\circ, 40^\circ, 45^\circ$, and incident shock-wave Mach numbers of $M_i = 1.55, 1.9, 2.3, 2.78$. One can see two examples: in Fig. 1 for $\theta_w = 30^\circ, M_i = 1.9$ and in Fig. 3 for a constant wedge angle of $\theta_w = 40^\circ$ and for all four M numbers.

It is evident that, as the gas on two sides of the SS flows away from the triple point, the SS thickness linearly increases. A density profile is evident through the increasing spacing between the fringes along the SS. Notice that, as predicted by the model, the spread angle increases with increasing Mach number. In order to quantitatively analyze the model predictions, a detailed comparison of the measured and predicted spread angles was done for all Mach numbers. Spread angle measurements were taken between two straight lines bounding the SS thickening region, as demonstrated in Fig. 3(b). Error estimates were set according to half the thickness of a single fringe. The results are plotted in Fig. 2 as a function of the incident shock-wave Mach number for reflecting wedge angles of $\theta_w = 20^\circ, 30^\circ, 40^\circ, 45^\circ$. Additional experiments conducted at a higher initial pressure of 100 kPa and at an incident Mach number of $M = 1.5$ are also plotted.

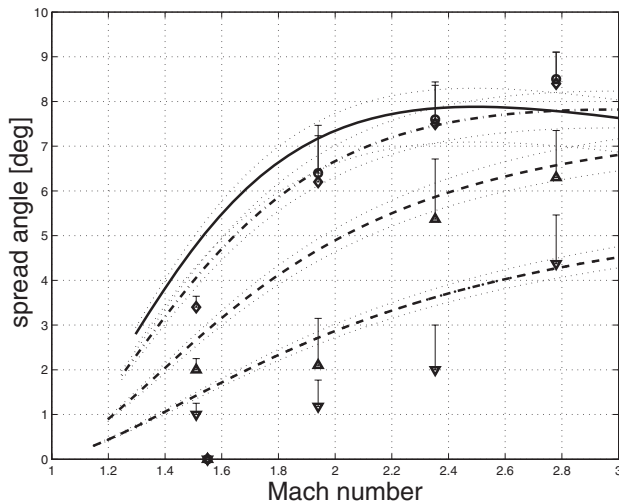


FIG. 2. SS instability spread angle as a function of incident shock-wave Mach number. Theoretical predictions in thick lines: $\theta_w = 45^\circ$ (solid line), $\theta_w = 40^\circ$ (dashed-dotted line), $\theta_w = 30^\circ$ (upper dashed line), and $\theta_w = 20^\circ$ (lower dashed line). Thin lines around the thick lines mark the error in the model prediction [see Eq. (1)]. Experimental results and error bars are also plotted; (○), (◇), (△), and (▽) mark experiments conducted with $\theta_w = 45^\circ, 40^\circ, 30^\circ$, and 20° , respectively. All of the experiments were conducted with ambient air at $P_0 = 10.1$ kPa, apart from the $M = 1.5$ experiments conducted at $P_0 = 100$ kPa.

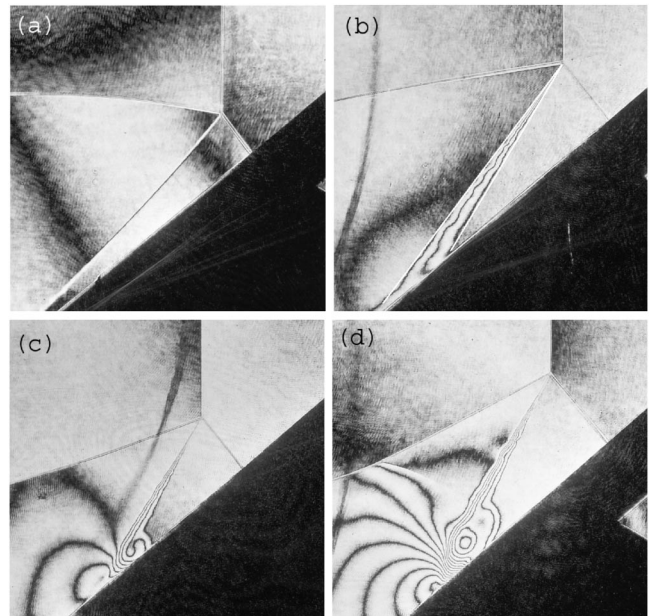


FIG. 3. Holographic interferometry images for MRs with a wedge angle of $\theta_w = 40^\circ$ and incident shock-wave Mach numbers of $M_i = 1.55$ (a), 1.9 (b), 2.3 (c), and 2.78 (d). Two white lines in (b) bound the SS, demonstrating the growth angle measurement technique.

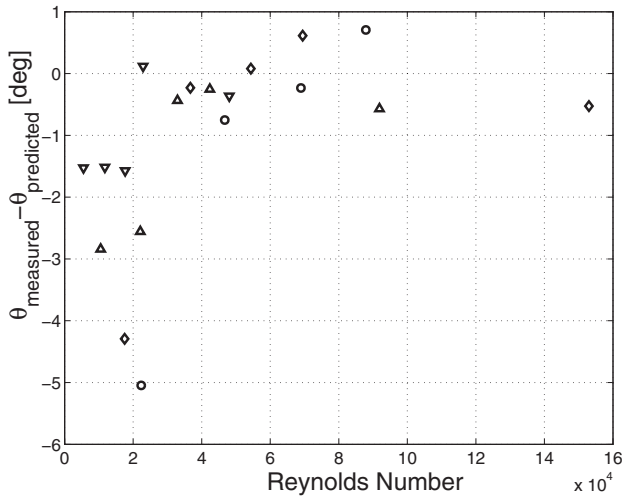


FIG. 4. Predicted spread angle subtracted from the measured spread angle, as a function of the SS Re number. (O), (◇), (△), and (▽) mark experiments conducted at $\theta_w = 45^\circ$, 40° , 30° , and 20° , respectively. Experiments conducted at an initial pressure of 100 kPa resulted in Re numbers of $\text{Re} = 15.3 \times 10^4$, 9.2×10^4 , and 4.8×10^4 for $\theta_w = 40^\circ$, 30° , and 20° , respectively.

In the figure, good agreement is demonstrated, apart from the following experiments at $P_0 = 10.1$ kPa: all the Mach 1.55 experiments, the $\theta_w = 30^\circ$ experiments at $M < 2$, and the $\theta_w = 20^\circ$ experiments at $M < 2.4$. In order to understand the cause for the above disagreements, the discrepancy between the model predictions and the experimental results is plotted in Fig. 4 against the SS shear velocity Re number. The Re number is calculated according to $\text{Re} = \frac{\Delta v l}{\nu}$, where Δv is the shear velocity, ν is the average ideal gas kinematic viscosity calculated at regions 2 and 3 according to $\nu_{\text{air}} = (181.92 + 0.536T)/\rho$ [11], and l stands for a typical length scale of 1 cm (chosen according to the typical size of the Mach stem).

From the figure, it is clear that all of the experiments conducted at $\text{Re} > 2 \times 10^4$ show good agreement with theory. Special attention should be pointed out to experiments conducted at $M = 1.55$ with $P_0 = 10$ kPa where no spread angle could be measured, whereas similar $M = 1.5$ experiments but with $P_0 = 100$ kPa show very good agreement. For the $\theta_w = 45^\circ$ experiments, for example, the resulting physical properties of regions 2 and 3 are $\rho_2 = 0.4$ kg/cm³, $\rho_3 = 0.36$ kg/cm³, $v_2 = 412$ m/sec, $v_3 = 257$ m/sec, and $a = 460$ m/sec for the $P_0 = 10$ kPa experiment and $\rho_2 = 3.8$ kg/cm³, $\rho_3 = 3.5$ kg/cm³, $v_2 = 402$ m/sec, $v_3 = 257$ m/sec, and $a = 454$ m/sec for the $P_0 = 100$ kPa experiment, both leading to a very similar spread angle according to Eq. (1). The important difference between the two classes of experiments are the higher densities obtained at the $P_0 = 100$ kPa experiments, introducing weaker kinematic viscosities and larger Re numbers (see caption of Fig. 4).

Together with Fig. 4, it is clear that the disagreements between the model and the experiments are due to viscosity effects, which are not accounted for in Eq. (1). Viscosity effects, serving as a secondary mix cutoff stabilizing mechanism (through a cutoff Re number), are a well known phenomenon. The critical Re number, measured at 2×10^4 , is similar to critical Re numbers demonstrated for several other mixing phenomena, such as secondary mixing at the Richtmyer-Meshkov and KH instabilities [2,3].

Summary.—It is shown that, from the properties of a large-scale hydrodynamic phenomena, i.e., densities, viscosities, velocities, and average sound speed, one can predict the existence and width of a secondary small-scale turbulent mixing zone through a simple analytical procedure based on models of large-scale KH instability growth. Using this technique, the evolution of the MR SS instability was analytically characterized. Good agreement is achieved with an experimental evaluation of the SS spread angle, conducted at Mach numbers of $M_i = 1.5$ – 2.78 and spread angles of $\theta_w = 20^\circ$ – 45° . A critical Re number of 2×10^4 is found to distinguish between turbulent and laminar flows, thus indicating secondary turbulent mixing generated through the evolution of the KH instability as the cause for the SS discontinuity thickening. The success in modeling secondary mixing using large-scale models of the KH instability should provide a guideline for future research in secondary turbulent mixing phenomena.

The financial support of the Interdisciplinary Shock-Wave Research Center of the Institute of Fluid Science, Tohoku University, for conducting the experimental phase of the presented research and helpful discussions with D. Oron are acknowledged by the authors.

-
- [1] S. P. Regan *et al.*, Phys. Rev. Lett. **89**, 085003 (2002).
 - [2] Y. Zhou, H. F. Robey, and A. C. Buckingham, Phys. Rev. E **67**, 056305 (2003).
 - [3] P. E. Dimotakis, J. Fluid Mech. **409**, 69 (2000).
 - [4] G. Ben-Dor, *Shock Wave Reflection Phenomena* (Springer-Verlag, Berlin, 1992).
 - [5] J. von Neumann, Navy Department, Bureau of Ordnance, Washington, DC, Explosives Research Report No. 12, 1943.
 - [6] G. L. Brown and A. Roshko, J. Fluid Mech. **64**, 775 (1974).
 - [7] A. Rikanati, U. Alon, and D. Shvarts, Phys. Fluids **15**, 3776 (2003).
 - [8] S. A. Ragab and J. L. Wu, Phys. Fluids A **1**, 957 (1989).
 - [9] H. Li and G. Ben-Dor, J. Fluid Mech. **341**, 101 (1997).
 - [10] F. Ohtomo, K. Ohtani, and K. Takayama, Shock Waves **14**, 379 (2005).
 - [11] *American Institute of Physics Handbook*, edited by Dwight E. Gray (McGraw-Hill, New York, 1972).